

EFFECTS OF GROUNDWATER FLUCTUATION ON GEOENVIRONMENTAL CONTAMINATION

GIANCARLO FLORES¹, TAKESHI KATSUMI¹, TORU INUI²

¹Graduate School of Engineering, Kyoto University, Kyoto, Japan

²Graduate School of Global Environmental Studies, Kyoto University, Kyoto, Japan

ABSTRACT: The alteration of weather patterns due to climate change is affecting not only the historical levels of the oceans, but also of groundwater tables. Therefore, the importance of a correct understanding of the behavior of contaminants in the subsurface due to fluctuating groundwater conditions is not only evident, but urgent. In this paper we describe a new *Simplified Image Analysis Method* developed to assess the behavior of *Non-Aqueous Phase Liquids* (NAPLs) in granular soils when subject to fluctuating groundwater conditions. This new method, based on a derivation from the Beer-Lambert Law of Transmissivity, is used to determine the saturation distribution of water (S_w) and NAPL (S_o) in three-phase (air-water-NAPL) two-dimensional domains, by replacing the average optical density values calculated at two different wavelengths ($\lambda = 450$ nm and 640 nm) in the linear regression equations obtained for each matrix element of the tested domain, and solving for S_w and S_o . The two regression equations are obtained after the analysis of photographs of the domain taken at the two aforementioned wavelengths under each of the following three limit conditions: a) $S_w = 100\%$, $S_o = 0\%$; b) $S_w = 0\%$, $S_o = 100\%$; and c) $S_w = S_o = 0\%$. The *Simplified Image Analysis Method* was then used to analyze the behavior of three different fluctuating groundwater systems, a two-phase air-water column system, a three-phase air-water-NAPL column system, and a three-phase air-water-NAPL tank. Results show that this non-intrusive and non-destructive method is reliable in providing water and NAPL saturation distributions throughout the domain when studying the effects of porous soil contamination by NAPLs subject to dynamic conditions.

INTRODUCTION

When released to the vadose zone, *Light Non-Aqueous Phase Liquids* (LNAPLs), such as petroleum derivatives and others, can pose significant contamination risks to the groundwater. To remediate these releases in an efficient and cost-effective way, remediation works should be guided by field data that should be on itself interpreted by numerical models using the appropriate assumptions. To verify the accuracy of these mathematical and computational models, laboratory tests should be prepared and run to obtain precise saturation information, especially under the dynamic conditions usually present in nature. This study introduces a *Simplified Image Analysis Method* as a tool to measure water and light non-aqueous phase liquids (LNAPLs) saturation distributions in whole three-phase 2D domains, when evaluating the effects of groundwater fluctuations on LNAPL migration in porous media.

IMAGE ANALYSIS

The Beer-Lambert Law of Transmittance states that when a beam of parallel monochromatic radiation with power I_0 strikes a block of absorbing matter perpendicular to a

surface (Fig. 1), after passing through a length b of the material, which contains n absorbing atoms, ions or molecules, its power is decreased to I_t as a result of absorption:

$$\log_{10} \frac{I_0}{I_t} = \epsilon bc = D_t \quad (1)$$

where I_0 is the initial radiant power, I_t the transmitted power, ϵ a numerical constant, b the length of the path, c the number of moles per liter of absorbing solution, and D_t the optical density (Skoog et al. 2007).

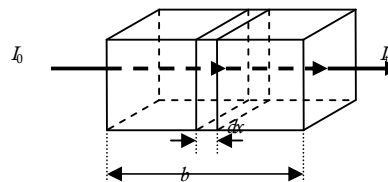


Figure 1 Radiation I_0 is attenuated to I_t by a solution of absorbing solution

When a photographic film is subjected to light and developed, the exposed grains of silver halides are changed into metallic silver which creates a change in the light transmittance of the film (Iizuka 1987). The transmittance τ defines how much light is transmitted through the photographic negative and can be written as:

$$\tau = \frac{I_t}{I_0} \quad (2)$$

where I_t and I_0 are the transmitted and incident luminous intensities, respectively. In digital photography, RAW files are the equivalent to photographic films, and the pixel value is the equivalent to the transmitted light through a negative grain.

Optical density D_t is related to the transmittance as:

$$D_t = -\log_{10}(\tau) \quad (3)$$

The value $D_t = 0$ or unit transmittance is the analogue for the reflectance of an ideal white surface (Gold & Asher 1976).

For digital images, the average optical density D_i is defined for the reflected light intensity as:

$$D_i = \frac{1}{N} \sum_{j=1}^N d_{ji} = \frac{1}{N} \sum_{j=1}^N \left(-\log_{10} \left(\frac{I_{ji}^r}{I_{ji}^0} \right) \right) \quad (4)$$

where N is the number of pixels contained in the area of interest and, for a given spectral band i , d_{ji} is the optical density of the individual pixels, I_{ji}^r is the intensity of the reflected light given by the individual pixel values, and I_{ji}^0 is the intensity of the light that would be reflected by an ideal white surface (Kechavarzi et al. 2000).

For a sample of thickness x , and using the definition of transmittance (Eq. (1) and (2)), the Beer-Lambert Law of Transmittance can be rewritten as:

$$\tau = e^{-acx} \quad (5)$$

where τ is the transmittance of a solution of unit concentration, a the absorption coefficient, c the concentration of a dye, and x the thickness of the medium (MacAdam 1981). Calculating logarithms of Eq. (5) and using Eq. (3) we get:

$$D_t = c \cdot D_0 \quad (6)$$

where D_0 is the optical density of a solution of unit concentration, and D_t the optical density of a solution of

concentration c . Equation (6) shows that optical density is linearly correlated to dye concentration, as was experimentally corroborated by Kechavarzi et al. (2000) and by Flores et al. (2009a, b).

When two cameras with two different band-pass filters (wavelengths $\lambda = i$ and j) are used, and when water and NAPL are mixed with dyes whose predominant color wavelengths are also i and j , we obtain two different sets of linear equations that can be solved for S_w and S_o :

$$\begin{cases} D_i = a \cdot S_w + b \cdot S_o + c \\ D_j = d \cdot S_w + e \cdot S_o + f \end{cases} \quad (7)$$

This is the base of the *Multispectral Image Analysis Method*: the calculation of two correlation equations via calibration tests using small samples and their subsequent use to determine water and NAPL saturation values (S_w and S_o) on larger three-phase (air/water/NAPL) domains (Kechavarzi et al. 2000).

SIMPLIFIED IMAGE ANALYSIS METHOD

The Multispectral Image Analysis Method relies on the use of different band-pass filters—flat by design—to allow digital cameras to capture the light reflected by the studied system on one particular wavelength each. Since these band-pass filters are designed for parallel light, they behave in a different way according to the angle of incidence of the reflected light (Fig. 2).

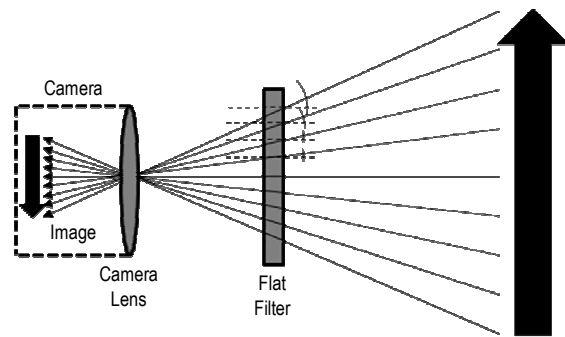


Figure 2 Effect of variable angle of incidence of reflected light on flat band-pass filters

Noting that the relative position between the camera and the domain remains constant, the different angles of incidence for the reflected light are also constant for the duration of the tests. It could be assumed that instead of one there exist dozens of small (and different) band-pass filters that remain fixed on position for the whole duration of the test, requiring the preparation of a different set of calibration equations for each small assumed band-pass filter, which is unpractical. Hence,

the need to develop a simplified version of the Multispectral Image Analysis Method.

Observing that each Eq. (7) represents a plane, and that only three non-collinear points are needed to define one, a careful choice of points will provide the needed set of equations for each mesh element. For these studied conditions, the best points are those located in the extremes of the plane (Fig. 3):

- $S_w = 0\%$; $S_o = 0\%$ Dry Sand
- $S_w = 0\%$; $S_o = 100\%$ LNAPL Saturated Sand
- $S_w = 100\%$; $S_o = 0\%$ Water Saturated Sand

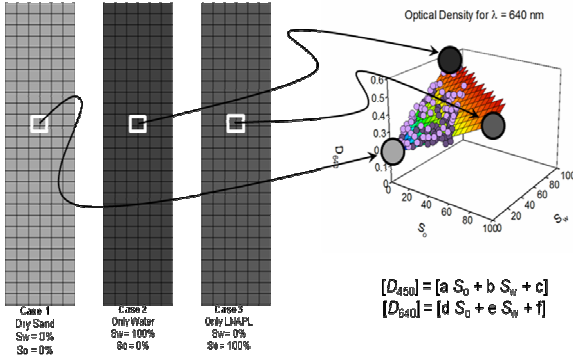


Figure 3 Each element of the mesh yields a unique set of regression equations

If the domain is filled with sand under each limit condition, and later photographed, all elements of the matrix will share the same conditions. The average optical density values for each mesh element of the studied domain could then be calculated and compared to the corresponding ones for all three cases, and a matrix of correlation equation sets could be obtained, each one corresponding to each mesh element (Eq. 8):

$$\begin{bmatrix} D_i \\ D_j \end{bmatrix}_{mn} = \begin{bmatrix} (D_i^{10} - D_i^{00}) \cdot S_w + (D_i^{01} - D_i^{00}) \cdot S_o + D_i^{00} \\ (D_j^{10} - D_j^{00}) \cdot S_w + (D_j^{01} - D_j^{00}) \cdot S_o + D_j^{00} \end{bmatrix} \quad (8)$$

where m and n are the dimensions of the matrix, $[D_i]_{mn}$ and $[D_j]_{mn}$ are the values of average optical density of each mesh element for wavelengths i and j ; $[D_i^{00}]_{mn}$ and $[D_j^{00}]_{mn}$ are the average optical density of each mesh element for dry sand; $[D_i^{10}]_{mn}$ and $[D_j^{10}]_{mn}$ for water saturated sand; and $[D_i^{01}]_{mn}$ and $[D_j^{01}]_{mn}$ for NAPL saturated sand. Since each mesh element has its own pair of correlation equations that already accounts for both the variable behavior of the band-pass filters and for the spatial variation of light, the use of image subtraction is not needed and one extra source of error is eliminated (Flores et al. 2010).

COLUMN TEST: WATER DRAINAGE

Equipment and Materials

A $3.5 \times 3.5 \times 50$ cm one-dimensional column with a transparent glass-wall (Fig. 4) was designed to study the behavior of lowering groundwater table in a Toyoura sand (particle density $\rho = 2.65$ g/cm³, equivalent grain size $D_{60} = 0.196$, void ratio $e = 1.1$) one-dimensional column with the aid of the *Simplified Image Analysis Method*. This column and tests are similar to those by Kamon *et al.* (2007), but the column was square ($\phi = 3.5$ cm) instead of circular ($\phi = 3.5$ cm) to minimize the optical distortion when taking digital photographs.

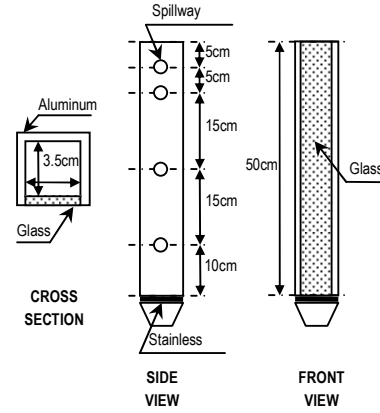


Figure 4 Column design

A consumer grade digital camera (Nikon D70s) with a 450 nm band-pass filter was used to photograph the column. The sole lighting sources were two 500 W floodlights in the dark room, and a Gretagmacbeth white balance card was located next to the column to provide a constant white reference. An external water tank was connected to the column to control the water table height (Fig. 5). To facilitate observations, the water was blue-dyed with Brilliant Blue FCF (1:10000), a dye that is not absorbed by the soil particles.

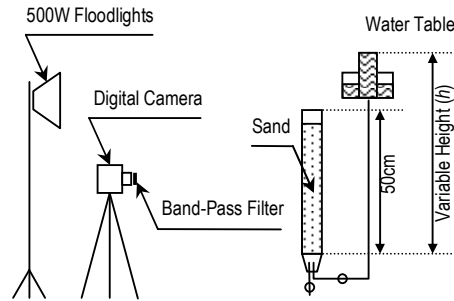


Figure 5 Column system design

Calibration

This test required two calibration photographs: the studied column filled with dry sand and the column filled with water saturated sand. Because only water was used, we can focus on one side of the regression plane ($S_o = 0\%$) shown in Fig. 2. Hence, Eq. (8) can be reduced to:

$$[D_{450}]_{mn} = \left[(D_{450}^{10} - D_{450}^{00}) \cdot S_w + D_{450}^{00} \right]_{mn} \quad (9)$$

where m and n are the dimensions of the matrix. $[D_{450}]_{mn}$ is the value of the average optical density of each mesh element for a wavelength of 450 nm. $[D_{450}^{00}]_{mn}$ is the average optical density of each mesh element for dry sand. $[D_{450}^{10}]_{mn}$ is the average optical density of each mesh element for water saturated sand.

Experiment

The column was initially filled with fully water saturated Toyoura sand. The sand was previously saturated with blue-dyed water and left overnight in a vacuum chamber to ensure it was completely saturated. Then the saturated sand was slowly poured with the help of a spoon in the column filled with de-aired water, and compacted with an aluminum bar every 2-3 cm. The external water tank, initially located at $h = 45$ cm, was quickly lowered to $h = 5$ cm, and the water inside the column was drained for 60 hours. To avoid producing a vacuum, the top of the column was open. Digital pictures were taken every hour. The camera was set to manual mode, and the aperture, shutter speed, and white balance were defined and maintained constant throughout the experiment. The camera was remotely controlled (using Nikon Camera Control Pro 2 software) to avoid vibrations and camera displacement. The two 500 W floodlights were turned on 30 seconds prior to taking the pictures and turned off right after that to avoid fluctuations in the column's temperature. Room temperature was kept at 20 °C and humidity at 70%.

Computational Analysis

All pictures were exported from the NEF format (Nikon proprietary RAW version files) to the TIFF format (Tagged Image File Format) using Nikon ViewNX 1.5.0. TIFF images were analyzed with an ad-hoc program written in MATLAB 2007a to obtain $[D_{450}]_{mn}$.

As previously mentioned, because NAPL was not infiltrated during this test, $S_o = 0\%$, and the simplified Eq. (9) was used.

The $[D_{450}]_{mn}$ matrix is calculated for each picture taken during the test so that the water saturation matrix $[S_w]_{mn}$, which corresponds to each picture, can be solved. Figure 6 plots the $[S_w]_{mn}$ values for $t = 0, 30,$ and 60 hr.

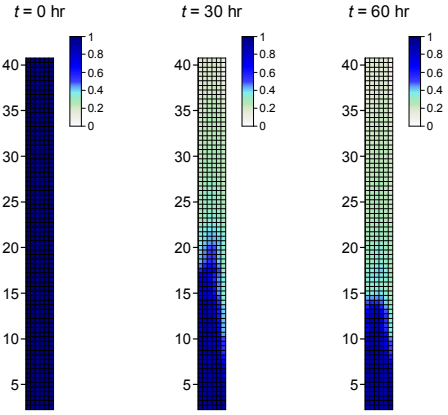


Figure 6 Water saturation distribution matrices $[S_w]_{mn}$ for $t = 0, 30$ and 60 hr

Although Fig. 6 shows the water distribution in the entire domain at three specific instances during the experiment ($t = 0, 30,$ and 60 hr), in all, we obtained 61 similar water distribution graphics (not shown here) because data was collected one an hour throughout the 60 hour test. Instead of showing all 61 pictures, we analyzed the dynamic behavior of the water column by examining a Water Saturation vs. Time plot for areas of the column located at different heights (Fig. 7).

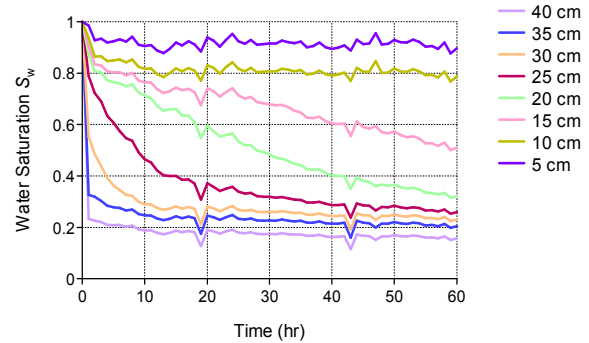


Figure 7 Water Saturation vs. Time at different heights

Each line in Fig. 7 corresponds to the behavior of the water saturation in the column at a specific height with time and, since the water head is known (water table height = 5 cm), we can also plot the Saturation – Water Head pairs corresponding to each time and height. Figure 8 plots the saturation-water head pairs corresponding to $t = 0, 10, 20, 30, 40, 50,$ and 60 hr.

Our analysis indicated that 128.17 g of water drained from the column. In fact, 117.45 g was recovered from the external tank, yielding a difference of 9.1% (Table 1).

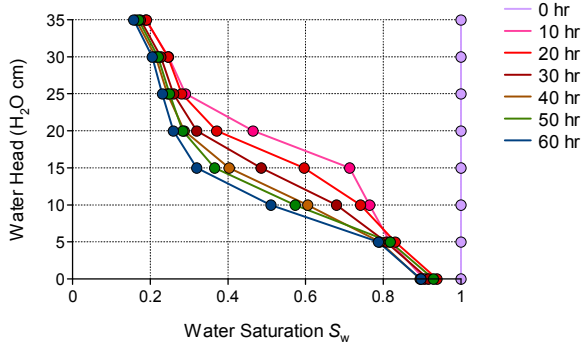


Figure 8 Variation of the Saturation – Water Head relation with time

Table 1 Drained water mass balance, comparison between calculated and measured

Water in the Column	Real	Computed
W_w at $t = 0$ hr	NA	216.68 g
W_w at $t = 60$ hr	NA	88.51 g
Drained water	117.45 g	128.17 g
Difference (mass)		10.72 g
Difference (%)		9.1%

Discussion

The first experiment tested the simplified image analysis method for a two-phase case (air/water). The lack of the third phase allowed Eq. (8) to be simplified, but the overall method remained the same. Similar to previous experiments (data not shown), the image analysis method is extremely sensitive to variations in lighting conditions; thus, efforts were made to maintain constant conditions.

Figure 6 depicts the water distribution inside the column at three different times, and shows that despite our efforts to create a uniformly compacted volume of sand, preferential paths were created at the corners of the square-shaped cross section of the column (Fig. 4), which are apparent because the water front receded faster away from the center of the column. Although this is an undesired behavior, it illustrates how the *Simplified Image Analysis Method* is capable of showing differences in water saturation by calculating the saturation distribution in the entire domain with high detail, especially compared to other methods that measure saturation at specific points (e.g., electrical conductivity probe, gamma ray attenuation, etc), typically along the center and assume that the saturation front recedes uniformly with height.

Figure 7 shows the dynamic behavior of water with time as well as how the receding water front is displaced faster at the beginning of the experiment, and then slowly stabilizes. Once the water saturation (S_w) became close to 15%, it remained there for the duration of the experiment.

This value is called *Residual Saturation*, and the value for the most extreme condition (when $h = 40$ cm) of 15.7%, is close to the results obtained by Li (2005), which was 14.5% for an air-water system following the van Genuchten model. Figure 8 shows the displacement of the saturation-water head relation, which is close to the S - p relation, with time. The larger the water head, the faster a stabilized condition was achieved.

Finally, although the difference between the calculated amount of water that drained from the column (obtained using our simplified method) and the real amount of water recovered is less than 10%, because the external tank (the one that recovered the drained water) was open to the room during the 60 hour experiment, it is possible that some of the water evaporated (even under the controlled temperature and humidity conditions maintained in the room). Thus, the real difference may be less than the calculated 9.1%. To reduce this potential error, two measures were taken in the subsequent experiment; (i) a closed system to minimize the amount of evaporation from the drained water and (ii) paraffin liquid, a non-volatile LNAPL for the mass-balance comparison fluid were used.

COLUMN TEST: WATER/LNAPL FLUCTUATION

Equipment and Materials

The same $3.5 \times 3.5 \times 50$ cm one-dimensional column with a transparent glass-wall designed for the previous test (Fig. 4) was used to study the behavior of an LNAPL, affected by a fluctuating groundwater table, in a Toyoura sand (particle density $\rho = 2.65$ g/cm³, equivalent grain size $D_{60} = 0.196$, void ratio $e = 1.1$) one-dimensional column with the aid of the *Simplified Image Analysis Method*. The wetting fluid was blue-dyed water (Brilliant Blue FCF, 1:10000) and the non-wetting fluid was red-dyed paraffin liquid (Sudan III, 1:10000), a LNAPL. A specific setup was devised for the top part of the column to keep it fully saturated during the first hour of the test (Fig. 9).

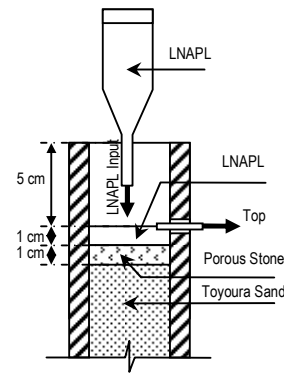


Figure 9 Setup of the top part of the column

Calibration

This test required three calibration pictures with each camera: each camera took a picture of the column filled with dry sand, with water saturated sand, and with LNAPL saturated sand. These six pictures correspond to $[D_{450}^{00}]_{mn}$, $[D_{450}^{10}]_{mn}$, $[D_{450}^{01}]_{mn}$, $[D_{640}^{00}]_{mn}$, $[D_{640}^{10}]_{mn}$, and $[D_{640}^{01}]_{mn}$.

Experiment

The column was initially filled with fully water saturated Toyoura sand, and topped with a 1 cm cap of LNAPL. The test was divided into four stages: first drainage ($t = 0$ to 72 hr), first imbibition ($t = 72$ to 120 hr), second drainage ($t = 120$ to 192 hr) and second imbibition ($t = 192$ to 240 hr).

First Drainage. The water tank was quickly lowered 65 cm from its original position to a height of $h = -20$ cm (20 cm below the bottom of the column), and the water inside the column was allowed to drain. During the first hour of the test, 28 g of LNAPL infiltrated the column from the top through the porous stone. Beginning in the second hour air was allowed to freely infiltrate the column through the same porous stone. The top of the column was open to avoid producing a vacuum effect. This stage took 72 hours.

First Imbibition. After the end of the first drainage, the water tank was quickly raised 112 cm to a height of $h = 92$ cm, and due to the upward water pressure, the water table inside the column moved up. The LNAPL that infiltrated into the column during the drainage process was displaced by the water and flowed out of the column through the top spillway. The top of the column was open to avoid producing overpressure. This stage took 48 hours.

Second Drainage. The water tank was lowered again to $h = -20$ cm, and the water and LNAPL present in the column were allowed to drain. No additional LNAPL was infiltrated into the column. This stage took 72 hours.

Second Imbibition. The water tank was raised once again to a height of $h = 92$ cm, and both water and the remaining LNAPL moved up due to the upward water pressure. The excess water and LNAPL flowed out of the column through the top spillway. This stage took 48 hours.

Two digital pictures of the column were taken simultaneously every hour using two cameras, one with a 450 nm band-pass filter and the other with a 640 nm band-pass filter. Both cameras were set to manual mode, and all the pictures were acquired with the same aperture, shutter speed, and white balance settings. The cameras were remotely controlled (using Nikon Camera Control Pro 2 software) to avoid vibrations and displacement. The two 500 W floodlights were turned on 30 seconds prior to taking each picture and turned off 30 seconds afterwards

to avoid changing the temperature of the column. Room temperature was maintained at 20 °C and humidity at 70%

Computational Analysis

All pictures were exported from NEF format (Nikon proprietary RAW version files) to TIFF format (Tagged Image File Format) using Nikon ViewNX 1.5.0. The TIFF images were analyzed with an ad-hoc program written in MATLAB 2007a.

Using the six calibration pictures, the average optical density matrices were calculated. $[D_{450}]_{mn}$ and $[D_{640}]_{mn}$ were calculated for each picture taken during the test, and the water and LNAPL saturation matrices ($[S_w]_{mn}$ and $[S_o]_{mn}$), which correspond to each picture, were solved. Figures 10 and 11 plot the $[S_w]_{mn}$ and $[S_o]_{mn}$ values for $t = 0, 72, 120, 192,$ and 240 hr for the first and second drainage and imbibition cycles, respectively.

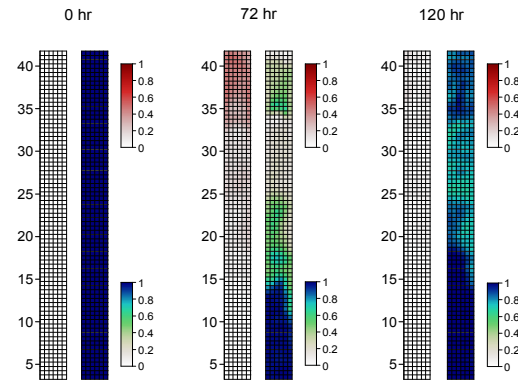


Figure 10 First drainage and imbibition. Blue plots (left) correspond to water saturation matrices $[S_w]_{mn}$ and red plots (right) to LNAPL $[S_o]_{mn}$

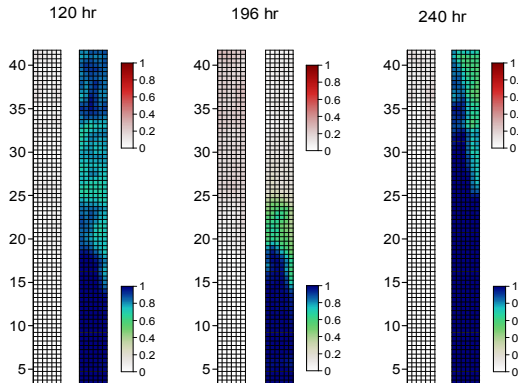


Figure 11 Second drainage and imbibition. Blue plots (left) correspond to water saturation matrices $[S_w]_{mn}$ and red plots (right) to LNAPL $[S_o]_{mn}$

Because the water and LNAPL saturation values do not necessarily total 100%, it would be impossible to plot

them together in the same graph. Thus, the column with time is represented by two graphs in Fig. 10 and Fig. 11: the left represents LNAPL saturation distribution $[S_o]_{mn}$ and the right represents water saturation distribution $[S_w]_{mn}$. Each pair should be considered together when studying the state of the column at a given time.

The dynamic behaviors of both the water and LNAPL fronts are better understood if S_w and S_o are plotted with time (Fig. 12 and Fig. 13).

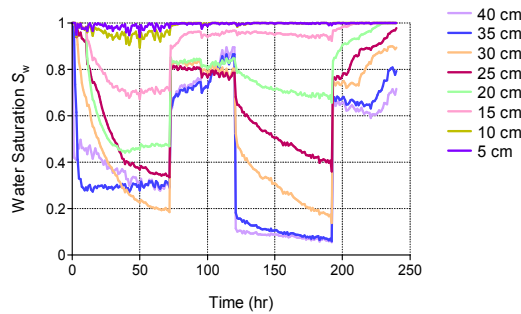


Figure 12 Water Saturation vs. Time

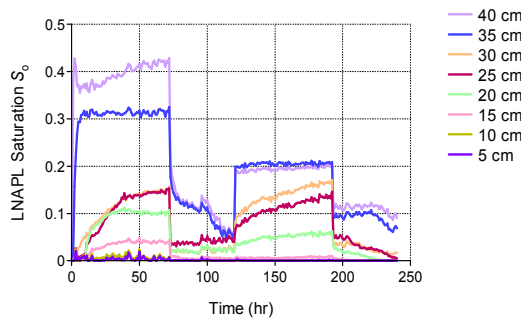


Figure 13 LNAPL Saturation vs. Time

According to the image analysis, after the two drainage and imbibition cycles of the original 28.00 g infiltrated during the first hour, 4.95 g of LNAPL remained in the column. Thus, 23.05 g should have been displaced out of the column. In fact, 22.02 g was recovered from the external tank, a difference of only 4.7% (see Table 2).

Table 2 Drained LNAPL mass balance, comparison between calculated and measured

LNAPL in the Column	Real	Computed
W_o at $t = 0$ hr	0.00 g	0.00 g
W_o at $t = 1$ hr	28.00 g	N/A
W_o at $t = 240$ hr	N/A	4.95 g
Drained LNAPL	22.02 g	23.05 g (28.00-4.95)
Difference (mass)		1.03 g
Difference (%)		4.7%

Discussion

This experiment tested the *Simplified Image Analysis Method* for a 1D three-phase case (air/water/LNAPL) under fluctuating conditions. Figures 10 and 11 show that the method can perceive and calculate minute amounts of LNAPL not easily observed with the naked eye. Paraffin liquid showed a typical LNAPL behavior under imposed fluctuating conditions; it initially migrated downward following the draining water until it reached a stable condition, and then it remained on the top part of the column even though the water table was 15-20 cm lower (Fig. 10, $t = 72$ hr). During the imbibition stage, raising the water table displaced part of the LNAPL, but some remained trapped within the column even though it should have floated over the water table (which was 50 cm above LNAPL) because LNAPL is less dense than water (Fig. 10, $t = 120$ hr). The second drainage-imbibition cycle displayed the same behavior and by the end of the experiment (Fig. 11, $t = 240$ hr) nearly 5 g or 18% of the original infiltrated 28 g remained trapped within the column below the water table.

The difference between the calculated amount of displaced LNAPL and the actual recovered LNAPL was only 4.7%, showing that the Simplified Image Analysis Method calculates saturation values with a precision of nearly 95%.

TANK TEST: WATER/LNAPL FLUCTUATION

Equipment and Materials

A 30×50×7.5 cm tank made of a transparent acrylic material was designed to study the behavior of LNAPL under the effects of a water table with a 2D displacement, vertical raise and horizontal flow, by using the described Simplified Image Analysis Method. The porous material was Toyoura sand (particle density $\rho = 2.65$ g/cm³, equivalent grain size $D_{60} = 0.196$, void ratio $e = 1.1$). Wetting fluid was blue-dyed water (water mixed with Brilliant Blue CFC, 10000:1 in mass) and non-wetting fluid was red-dyed paraffin liquid (paraffin liquid mixed with Sudan III, 10000:1 in mass).

Two digital cameras with two different band-pass filters ($\lambda = 450$ nm and 640 nm) were used to photograph the tank at $\Delta t = 1$ hr intervals. Two 500 W floodlights were installed in the dark room as sole lighting sources and a Gretagmacbeth white balance card was located next to the tank to provide for a constant white reference. The center tank compartment (30×50×7.5 cm) was filled with dry Toyoura sand ($S_w = 0\%$, $S_o = 0\%$) and the two lateral tank compartments (30×7.5×7.5 cm) were left empty and served to control both vertical groundwater displacement and horizontal flow. Both lateral tanks had five 1 cm holes separated 5 cm each to control the height of the water table at each side of the center tank. Two metallic meshes

were located between the center and lateral tanks to keep the sand in the experimental area and to allow for unrestricted water flow between the sides of the center tank and the lateral tanks (Fig. 14).

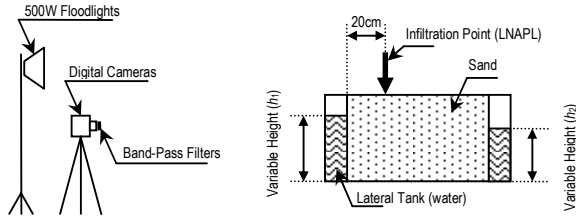


Figure 14 Tank system design

Calibration

For this test, three calibration pictures were needed with each camera: one of the tank filled with dry sand ($S_w = 0\%$, $S_o = 0\%$), one of the tank filled with water saturated sand ($S_w = 100\%$, $S_o = 0\%$), and one of the column filled with LNAPL saturated sand ($S_w = 0\%$, $S_o = 100\%$). In total we had six pictures corresponding to $[D_{450}^{00}]_{mn}$, $[D_{450}^{10}]_{mn}$, $[D_{450}^{01}]_{mn}$, $[D_{640}^{00}]_{mn}$, $[D_{640}^{10}]_{mn}$ and $[D_{640}^{01}]_{mn}$.

Experiment

The tank was filled with oven-dry Toyoura sand. The test was divided in 3 stages: LNAPL infiltration ($t = 0$ to 96 hr), imbibition first stage ($t = 96$ to 144 hr) and imbibition second stage ($t = 144$ to 192 hr):

LNAPL Infiltration. 167.25 g of red-dyed Paraffin Liquid were infiltrated at the point marked in Figure 1 via a $3 \times 7.5 \times 20$ cm prismatic transparent tube. The total volume completely infiltrated in approximately 5 hours, after which it continued to migrate downwards due to gravity forces. This stage took 96 hours.

Imbibition First Stage. After the end of the LNAPL Infiltration, the left lateral tank was filled with blue-dyed water to a height of $h_1 = 10$ cm, and a drainage point was opened at the right lateral tank at $h_2 = 5$ cm. This way, a differential of $\Delta h = 5$ cm was created that forced horizontal flow within the tank. No additional LNAPL was infiltrated into the tank. This stage took 48 hours.

Imbibition Second Stage. After the end of the Imbibition First Stage, the water level at the left lateral tank was raised to $h_1 = 20$ cm, and the drainage point at the right lateral tank was raised to $h_2 = 15$ cm. The differential of $\Delta h = 5$ cm was maintained so the horizontal flow was kept constant from the previous stage. No additional LNAPL was infiltrated into the tank. This stage took 48 hours.

Two digital pictures of the column were taken simultaneously every hour, each one with a camera using a 450 nm and a 640 nm band-pass filter. Both cameras were set to manual mode and all pictures were taken with the same aperture, shutter speed and white balance settings. The cameras were remotely controlled to avoid vibrations and displacement. The two 500 W floodlights were turned on 30 seconds before taking each picture and turned off 30 seconds after that, to avoid changing the temperature of the column. Room temperature was kept at 20 °C and humidity at 70%.

Computational Analysis

All pictures were exported from NEF format (Nikon proprietary RAW version files) to TIFF format (Tagged Image File Format) using Nikon ViewNX 1.5.0. The TIFF images were then analyzed with an ad-hoc program written in MATLAB 2007a. Using the six calibration pictures the average optical density matrices $[D_{450}^{00}]_{mn}$, $[D_{450}^{10}]_{mn}$, $[D_{450}^{01}]_{mn}$, $[D_{640}^{00}]_{mn}$, $[D_{640}^{10}]_{mn}$ and $[D_{640}^{01}]_{mn}$ were calculated and we obtained the matrix of correlation equations. $[D_{450}]_{mn}$ and $[D_{640}]_{mn}$ were calculated for each picture taken during the test, and then we solved for the

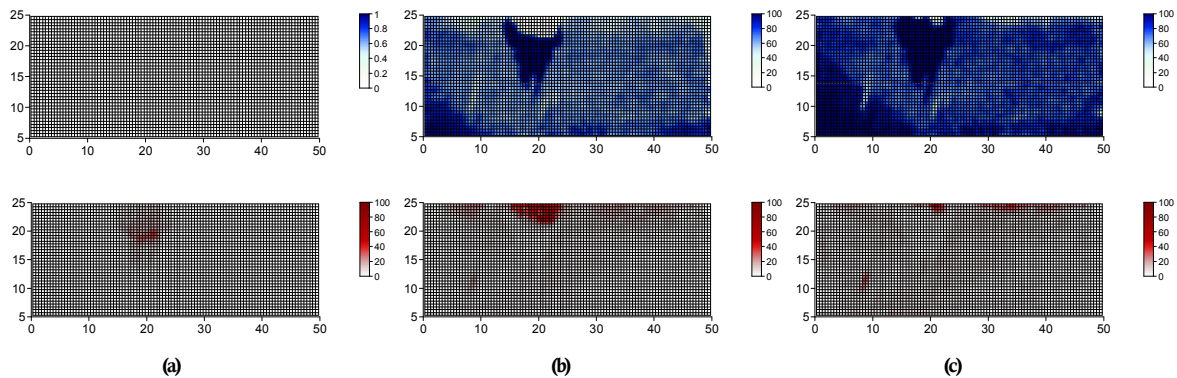


Figure 15 Saturation distribution at (a) $t = 96$ hr (end of infiltration), (b) $t = 144$ hr (end of imbibition first stage), and (c) $t = 192$ hr (end of imbibition second stage). Blue plots (top) correspond to water saturation matrices $[S_w]_{mn}$ and red plots (bottom) to LNAPL saturation matrices $[S_o]_{mn}$

water and LNAPL saturation matrices ($[S_w]_{mn}$ and $[S_o]_{mn}$) corresponding to each picture. $[S_w]_{mn}$ and $[S_o]_{mn}$ values for $t = 0, 48, 96, 144$ and 192 hr are graphically plotted in Fig. 15.

Since water and LNAPL saturation values are not necessarily complementary to 100%, it would be impossible to plot them both together in the same graphic. For this reason, in Fig. 15 we represent the state of the tank at each time with two graphics: one in red that represents LNAPL saturation distribution $[S_o]_{mn}$, and one in blue that represents water saturation distribution $[S_w]_{mn}$. Each pair of graphics should be considered together when studying the state of the column at any given time.

At the end of the test, four samples were carefully extracted from the tank, and their water and LNAPL saturation values were calculated using the Centrifuge Separation Technique. Results are shown in Table 3.

Table 3 Real vs. Calculated saturation values for samples taken from the tank at $t = 192$ hr

	S_w			S_o		
	Real	Calc.	Diff.	Real	Calc.	Diff.
1	0.092	0.096	+4.2%	0.803	0.812	+1.1%
2	0.070	0.065	-7.1%	0.809	0.836	+3.3%
3	0.223	0.239	+7.2%	0.677	0.705	+4.1%
4	0.023	0.025	+8.7%	0.938	1.000	+6.6%
5	0.015	0.016	+6.7%	0.910	0.992	+9.0%

Discussion

Paraffin liquid showed a typical LNAPL behavior under the imposed dynamic conditions: it first migrated downward due to gravity forces until it reached a stable condition, from which point it was vertically displaced by the capillary zone of the raising water table. As can be seen in Fig. 15 (b), even though water table was located at a maximum height of $h = 10$ cm (water table at the right side of the tank was just $h = 5$ cm), water displaced the LNAPL that was immobile in the zone between $h = 15$ cm and $h = 20$ cm, which means that it was the capillary zone the one that displaced it. Also in Fig. 15 (c) a similar behavior can be found, where LNAPL located between $h = 20$ cm and $h = 25$ cm is further displaced by the capillary zone caused by the new water table located at $h = 20$ cm (left side) and $h = 15$ cm (right side).

The vertical displacement of the LNAPL was fast enough not to allow for the horizontal water flow to greatly displace the trapped LNAPL. Only by comparison of Fig. 15 (a) and Fig. 15 (b) we can see how the LNAPL volume is slightly displaced to the right side when pushed upwards.

One factor that was not considered during the design of this tank test, and that showed an important influence to the experiment results, was that the LNAPL that was completely displaced upward from the porous soil

emerged on the surface, migrated laterally due to the groundwater horizontal flow, and contaminated the upper part of a larger area of the one that was subject to the LNAPL infiltration. This effect, that we call *Secondary Infiltration* and that can be seen in Fig. 15 (c) needs to be carefully understood by researchers working with mathematical models, which usually consider the soil surface as a boundary condition where the contaminant disappears as it leaves the soil, as these models will fail to predict the extra displacement reported here. As the Love Canal case showed (Colten & Skinner 1996), contaminants can be displaced upward and emerge above the soil surface due to vertical displacement of the groundwater, so the effects of the Secondary Infiltration on LNAPL contaminants needs to be addressed when analyzing areas that may have had a high water table at some time after the studied contamination occurred.

CONCLUSIONS

We have developed a novel *Simplified Image Analysis Method* to assess water and LNAPL saturation distributions in a porous media subject to fluctuating groundwater. This new method accounts for the effects of the variable angle of incidence of the reflected light that affects the response of the band-pass filters and eliminates the need to prepare the dozens of time-consuming samples required for standard calibration, saving on time and laboratory resources and improving its accuracy for points far from the center.

The *Simplified Image Analysis Method* increases the mathematical complexity of the computational analysis by providing not a single but a set of regression equations for the studied domain. This increase in complexity improves the accuracy of the method by providing each mesh element with its own set of non-related equations that account for both spatial variations of light and other surface imperfections.

Three column and tank tests were devised to verify the accuracy of the *Simplified Image Analysis Method* and to study the behavior of LNAPLs when subject to a fluctuating water table. Samples taken at the end of the test showed an error of less than 10%.

These tests allowed us to simulate different cycles of water drainage–imbibition in a porous soil such as those happening in sandy coastal areas due to tidal fluctuations, or in inland sandy areas due to groundwater fluctuation.

It was shown that, when spilled in a large enough quantity, LNAPLs, such as petroleum derivatives and others, will infiltrate the subsurface following the water table drainage while floating over it. Imbibition, however, can trap part of the LNAPLs below the water table (despite them having densities lighter than that of water) causing them to have a larger surface affected by horizontal water flow which, in turn, means that the

LNAPL can contaminate larger volumes of groundwater than before the imbibition stage of the cycle.

This should be specially taken into consideration when assessing, for example, the effects of petroleum leakage and spills on coastal petroleum depots, or of inland spills in sandy areas, as a large volume of LNAPL, contrary to common intuition, can be located below the water table as described here.

These experiments also confirmed that the *Simplified Image Analysis Method* can be used as a reliable technique to study LNAPL behavior on porous subsurface.

REFERENCES

- Colten C.E. and Skinner P.N. (1996). The road to Love Canal: managing industrial waste before EPA, Univ of Texas Pr.
- Flores G., Inui T., Katsumi T., Takatsukasa Y. and Kamon M. (2009a). Improvement of the precision of the image analysis method used as a tool to study LNAPL migration in porous media. *Proceedings of the International Joint Symposium on Geodisaster Prevention and Geoenvironment in Asia (JS-Fukuoka 2009)*. N. Yasufuku, K. Omine, T. Mukunoki and K. Kasama. Hanashoin, Fukuoka: 216-221.
- Flores G., Inui T., Katsumi T., Takatsukasa Y. and Kamon M. (2009b). Mechanism of Geoenvironmental Contamination with LNAPLs at Sites Close to the Ocean. *Nineteenth International Offshore and Polar Engineering Conference*. Osaka, Japan. 2: 323-329.
- Flores G., Katsumi T., Inui T. and Kamon M. (2010). Examination of LNAPL Migration in Porous Media Using a Simplified Image Analysis Method. *8th Japanese-Korean Seminar on Geo-Environmental Engineering*. Seoul, Korea: 83-90.
- Gold A. and Asher J.B. (1976). Soil Reflectance Measurement Using a Photographic Method. *Soil Sci Soc Am J* 40: 337-341.
- Iizuka K. (1987). *Engineering optics*. New York, Springer-Verlag.
- Kamon M., Li Y., Endo K., Inui T. and Katsumi T. (2007). Experimental study on the measurement of S-p relations of LNAPL in a porous medium. *Soils and Foundations*, 47(1): 33-45.
- Kechavarzi C., Soga K. and Wiart P. (2000). Multispectral image analysis method to determine dynamic fluid saturation distribution in two-dimensional three-fluid phase flow laboratory experiments. *Journal of Contaminant Hydrology* 46(3-4): 265-293.
- Li Y. (2005). Mechanism of LNAPL Migration in Conjunction with Groundwater Fluctuation. *Global Environmental Studies*. Kyoto, Kyoto University. Doctoral Degree: 167.
- MacAdam D.L. (1981). *Color measurement, theme and variations*. New York, Springer-Verlag.
- Skoog D.A., Holler F.J. and Crouch S.R. (2007). *Principles of Instrumental Analysis*. Belmont, CA, Thomsom Brooks/Cole.

